Physica Medica 136 (2025) 105060

Contents lists available at ScienceDirect

Physica Medica

journal homepage: www.elsevier.com/locate/ejmp

Technical Note

Decommissioning procedure and induced activation levels in the vault walls of a 11 MeV self-shielded Medical Cyclotron: simulations and measurements

Simone Manenti [a,b,*], Carlo Bergamaschi [c], Francesco Broggi [b], Andrea Ferrari [c], Flavia Groppi [a,b], Alessandro Loria [d], Massimiliano Nizzi [c], Antonella del Vecchio [d], Riccardo Calandrino [d]

[a] Department of Physics, University of Milan, Via Celoria 16, I-20133 Milano, Italy
[b] Laboratorio Acceleratori e Superconduttività Applicata (LASA), Department of Physics, University of Milan and INFN-Milan, Via F.lli Cervi 201, I-20090 Segrate, MI, Italy
[c] Campoverde s.r.l., Via Marco Fabio Quintiliano 31, I-20138 Milano, Italy
[d] Medical Physics Department, Ospedale San Raffaele Via Olgettina 60, I-20132 Milano, Italy

ARTICLE INFO

Keywords:
Cyclotron
Dosimetry
Exposure
Occupational
Waste management

ABSTRACT

This study outlines the decommissioning process of an 11 MeV self-shielded medical cyclotron operated for over 12 years at the Ospedale San Raffaele, Milano, Italy. A comprehensive analysis of neutron-induced activation in the vault walls was performed to guide safe demolition procedures. Using FLUKA Monte Carlo simulations and laboratory-based gamma and beta spectrometry, the activity of long-lived radionuclides, particularly ^{55}Fe, was evaluated across multiple wall depths. Results demonstrated that residual activity was primarily confined to the top 5 cm of the wall, with some samples exceeding the Italian clearance level of 1 Bq g^{-1} for ^{55}Fe. Occupational exposure to demolition staff was assessed via external dosimeters and internal contamination checks, with all values reported below regulatory limits. These findings confirm that while personnel are not at radiological risk, certain components and wall materials must be classified as low-level radioactive waste (LLRW) and require long-term storage.

1. Introduction

In September 2017, the 11 MeV CTI Cyclotron was shut down after more than 12 years of continuous operation, having started in January 2005, in isotope production at the Nuclear Medicine Department of Istituto di Ricovero e Cura a Carattere Scientifico (IRCCS) Ospedale San Raffaele – Milano, Italy. The above-mentioned cyclotron was a self-shielded, negative ion accelerator, accelerating H^- ions up to 11 MeV. The maximum allowable current was 80 μA, while the average beam current on target was 40 μA. The cyclotron was used mainly to produce ^{18}F and ^{11}C: the former by ^{18}O(p,n)^{18}F reaction, using a target of commercially available ^{18}O enriched water (^{18}O > 94 %), and the latter by ^{14}N(p,α)^{11}C, using a gaseous target mixture of ^{14}N + 1 %O_2. The production of ^{13}N (ammonia labelled with nitrogen) by means of ^{16}O(p,α)^{13}N was added in the recent past. The workload of the cyclotron over the course of its operational life could be estimated, on average, around a value of 400 μA·h·week^{-1}.

The increased high load clinical activity of the PET in Nuclear Medicine Department (approximately 40 patients per day in 2015) demanded an efficient and reliable radioisotope production system. At the end of 2017, due to a severe damage to the RF system, it was decided, to shut down this unit and to shift the daily production to the second cyclotron in use at the department. At that time a foreign company who expressed interest in acquiring the cyclotron for a complete revamping for its further use was found. This solution has strongly simplified all the concern related to the complete decommissioning of the cyclotron and its components leaving us the surveillance of the wall demolition and the moving out of the unit, after removal of its highest activated components (target and foils).

The cyclotron component analysis confirmed the presence of gamma and pure beta emitters, ^{22}Na, ^{54}Mn, ^{60}Co, ^{65}Zn, ^{207}Bi, ^{55}Fe, ^{63}Ni at different values activity concentration, depending on the positioning of

* Corresponding author at: Department of Physics, University of Milan, Via Celoria 16, I-20133 Milano, Italy.
E-mail address: simone.manenti@unimi.it (S. Manenti).

https://doi.org/10.1016/j.ejmp.2025.105060
Received 29 April 2025; Received in revised form 1 July 2025; Accepted 21 July 2025
Available online 24 July 2025

the sample point and on the alloy of the sampled part as referred in a previous paper [1].

Several published papers report data on the activation of beam transport components [2–6], of the cyclotron vault [7–12] or linear accelerator [13–16], and recently data have been published related to 11 MeV [1] and 18 Mev [17] cyclotron accelerators decommissioning with detailed results on the activation of the cyclotron.

This work is focused on the study and measurement of the activation induced in the cyclotron vault wall object of demolition for the cyclotron move out, in order to verify the accomplishments of the activation of the wall rubble with the Italian clearance levels [18]. We have primarily focused on ^{55}Fe, as we expect that long-lived pure beta emitters may play a dominant role in assessing the demolition rubble.

In this work, the contribution of pure beta-emitting radionuclides was measured for the first time.

2. Materials and methods

A simulation was conducted using a Monte Carlo code (FLUKA) on the wall to be demolished for the removal of the cyclotron and its shielding, and two sets of samples were taken as described in the following paragraphs.

The simulation and sampling were conducted exclusively on this wall, since it was the only one that was dismantled. The objective was to measure the residual activity within the concrete material to appropriately evaluate its disposal as radioactive waste.

2.1. FLUKA simulation

The FLUKA simulation was intended solely as a preliminary assessment and not as a predictive evaluation of the actual wall radioactivation. The purpose of the simulation was to obtain a preliminary estimate of the activity distribution.

Given the preliminary nature of the results intended to be obtained from the FLUKA simulation, the cyclotron was simplified by considering only the metallic component of the magnet (yoke) (Fig. 1).

The concrete used in the simulation is a modified version of the PORTLAND cement (Fig. 2) from the FLUKA library. The shielding of the cyclotron, on the other hand, consists of 60 parts by mass of the modified PORTLAND cement, 60 parts of Sand (Fig. 2), 35 parts of Polyethylene, and 1.5 parts of boron carbide (B4C).

The simulation was conducted using FLUKA 4-4.0 [19,20] and Flair 3.3-1 [21] and was performed with 3.3×10^{11} primary protons. An 11 MeV proton beam was simulated impacting a target of H_2O highly enriched in ^{18}O.

We used the standard defaults described under NEW-DEFAults and JEFF-3.3 as neutron library.

The activity produced in the regions of interest was estimated using the RESNUCLEi card in FLUKA. The results were then normalized based on the cyclotron beam current and operational time. Starting from the simulated production activity, the expected activity at the day of the experimental measurement was calculated by accounting for the decay time.

Neutron distribution simulations were performed using the USRBIN card. A Cartesian mesh with spatial steps of $\Delta x = 1$ cm, $\Delta y = \Delta z = 3$ cm was defined to score neutron fluence in the wall region.

The statistical uncertainties of calculation results were estimated by FLUKA by doing calculations in several batches and computing the standard deviation of the mean (we ran 11 cycles of 10^{10} primaries each in 3 spawns).

To enhance statistical precision in regions of interest for radionuclide production, importance biasing was applied using the BIASING card in FLUKA. Higher importance values were assigned to specific regions to increase particle tracking and interaction sampling in areas where activation estimates were required. This variance reduction technique significantly improved the efficiency of the simulation without compromising accuracy.

The simulation was performed using FLUKA installed on Ubuntu within a Windows 11 pro machine using the Windows Subsystem for Linux (WSL). The system was equipped with a 13th Gen Intel® Core™ i7-13800H processor running at 2.50 GHz and 64 GB of installed RAM and the average CPU time used to follow a primary particle was 3.8×10^{-6} s.

The number of the produced ^{55}Fe radionuclides per primary proton

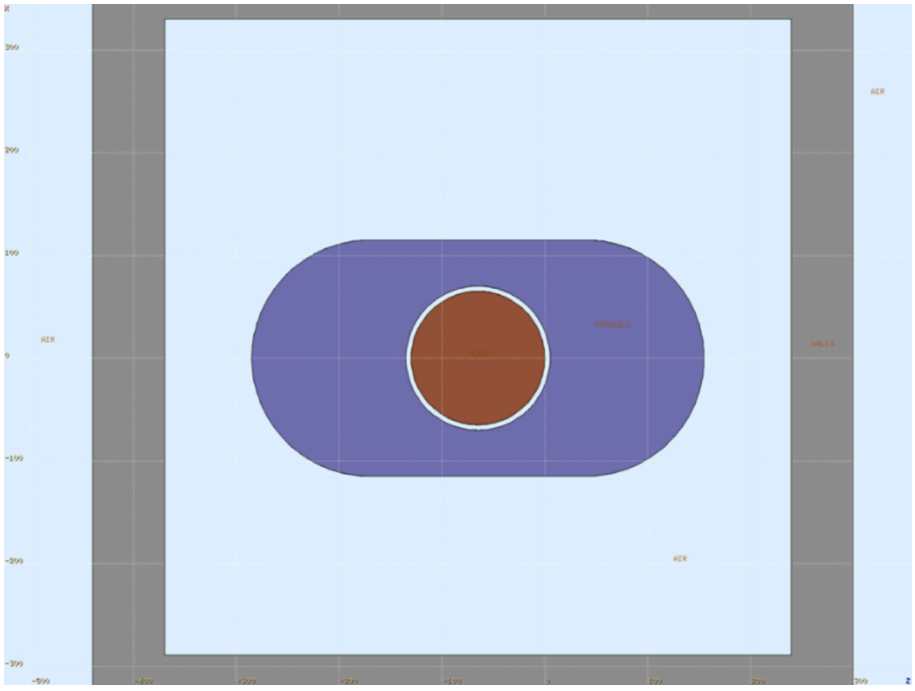

Fig. 1. Schematic representation of the cyclotron (brown), the shielding (violet) and the room. All dimensions are expressed in cm. (For interpretation of the references to colour in this figure legend, the reader is referred to the web version of this article.)

COMPOUND PORTLAND ▾ Mix: Mass ▾ Elements: 16..18 ▾

f1:	0.01	M1:	HYDROGEN ▾	f2:	0.001	M2:	CARBON ▾
f3:	0.52907997	M3:	OXYGEN ▾	f4:	0.016	M4:	SODIUM ▾
f5:	0.002	M5:	MAGNESIU ▾	f6:	0.033872	M6:	ALUMINUM ▾
f7:	0.337021	M7:	SILICON ▾	f8:	0.013	M8:	POTASSIU ▾
f9:	0.044	M9:	CALCIUM ▾	f10:	0.014	M10:	IRON ▾
f11:	8.8e-07	M11:	EUROPIUM ▾	f12:	1.29e-05	M12:	COBALT ▾
f13:	5e-07	M13:	TANTALUM ▾	f14:	1.25e-06	M14:	CESIUM ▾
f15:	1.15e-05	M15:	SCANDIUM ▾	f16:		M16:	▾
f17:		M17:	▾	f18:		M18:	▾

COMPOUND Sand ▾ Mix: Atom ▾ Elements: 10..12 ▾

f1:	0.135405	M1:	HYDROGEN ▾	f2:	0.004874	M2:	CARBON ▾
f3:	0.58389	M3:	OXYGEN ▾	f4:	0.012932	M4:	SODIUM ▾
f5:	0.022215	M5:	ALUMINUM ▾	f6:	0.226483	M6:	SILICON ▾
f7:	0.005179	M7:	POTASSIU ▾	f8:	0.004874	M8:	CALCIUM ▾
f9:	0.004146	M9:	IRON ▾	f10:		M10:	▾
f11:		M11:	▾	f12:		M12:	▾

Fig. 2. Composition of the modified PORTLAND cement and of the Sand used in the FLUKA simulation.

was simulated in four regions (Fig. 3) at different depths (0–5 cm, 5–10 cm, 10–15 cm, 15–20 cm, 20–25 cm, 25–30 cm, 30–40 cm, and 40–60 cm): the formation of ^{55}Fe was assessed in each of these layers.

The number of neutrons per primary proton (Fig. 3) is representative of the radioactivation caused by the neutrons within the wall.

2.2. Sampling and measurements

Two rounds of sampling and measurements have been taken at 9 and 20 points on a square 3 × 3 m^3 in the demolition area.

In the first phase, the analysis has been carried out sampling the concrete powder of a 30 cm depth drilling with a drill bit on nine sampling points (ID 1old–9old) and on a net as Fig. 4.

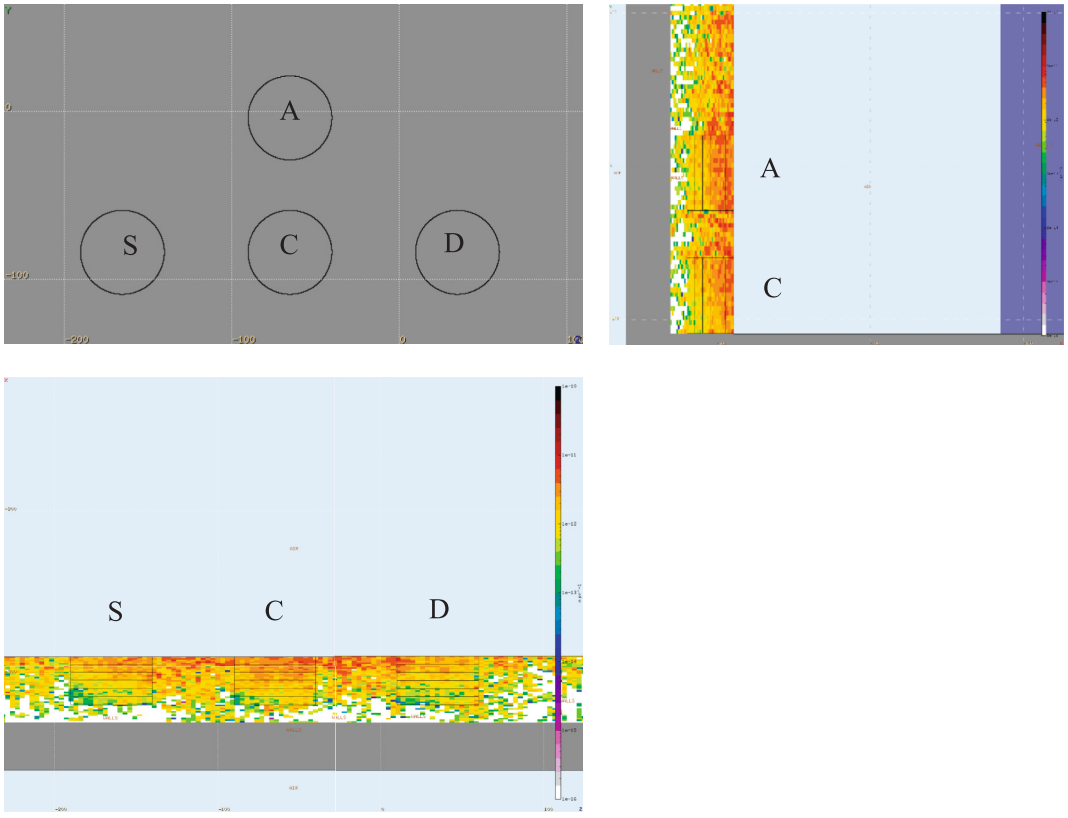

Fig. 3. Position of simulated sampling points in the wall adjacent to the self-shielded cyclotron and neutron flux per primary proton. All dimensions are expressed in cm.

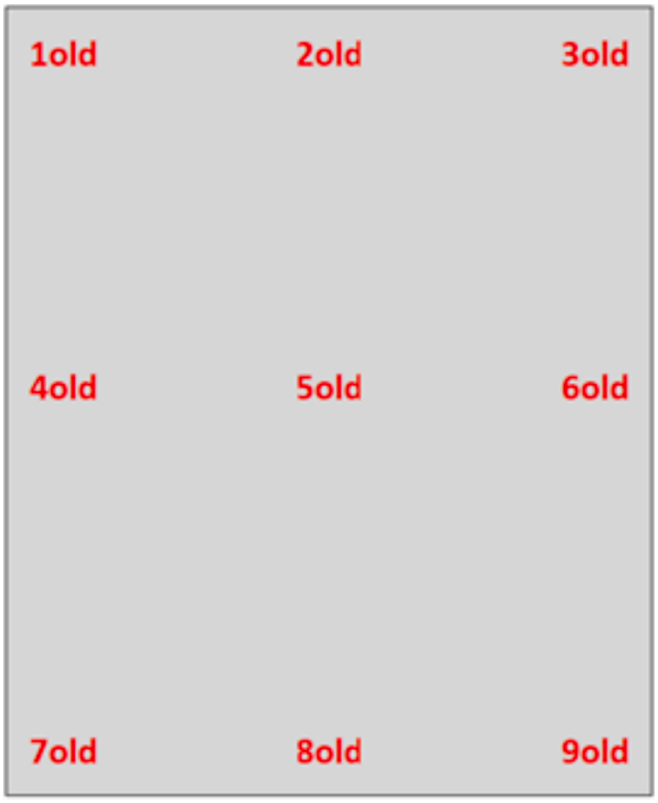

Fig. 4. First round sampling points.

The nine samples were firstly characterized by gamma spectrometry with HPGe and then a characterization by beta spectrometry of ^{55}Fe ^{63}Ni and ^{3}H was performed.

The gamma spectrometry was carried out using high-resolution High Purity Germanium (HPGe) detector (EG&G Ortec, 15 % relative efficiency, FWHM = 2.2 keV at 1.33 MeV) without any chemical processing.

The samples received were already in the form of a homogeneous powder inside 1 L Marinelli containers, ready to be measured in the correct geometry. The detector was calibrated with a certified liquid source of ^{152}Eu (CIS-DIAGNOSTICI S.P.A.) with an activity of 37 kBq ± 3.0 % as of 01/01/1995, using the same geometry as the samples. The low activity of the ^{152}Eu calibration source (~10 kBq), combined with moderate detector efficiency (15 %) and absence of sum peaks (e.g. 465 keV) in the spectrum, indicates that coincidence summing effects are negligible.

The measurement results were first corrected by subtracting the natural background counts and then adjusted for self-attenuation. In fact, in this study, calibration was performed using aqueous solutions (density ≈ 1.0 g cm^{-3}), which are typically considered weakly attenuating media for gamma radiation, especially at medium to high energies. However, the analysed samples consist of cementitious material with a density of 2.8 g cm^{-3}. Due to this higher density and potentially higher atomic number elements, these materials present increased photon attenuation. To account for this discrepancy, the spectrum analysis program (GammaVision, EG&G Ortec) provides a correction for self-absorption.

The results are reported with their respective errors, obtained through error propagation, considering uncertainties related to the calibration source, counting statistics (uncertainties on the net peak area), and the subtracted natural background.

Radiochemical separations were performed following analytical methods accredited by the laboratory. The procedures were based on Eichrom methodologies: Method No. FEW01, Analytical Procedure, Revision 1.1, May 1, 2014 [22] and Method No. NIW01, Analytical Procedure, Revision 1.3, May 1, 2014 [23].

Sample dissolution was carried out using a microwave mineralization system: to obtain a suitable sample for LSC analysis the concrete samples were dissolved in an acidic mixture of HNO_3, HCl, and H_3PO_4 by a digestion process in a digestion system (Milestone Ethos UP), with the addition of a small amount of hydrofluoric acid (HF) to enhance the digestion process.

The dissolved sample was then dried on a heating plate for three times adding a few amounts of HCl. The final sample (a solution 1 M HCl) is then counted in LSC for the gross beta measurement.

For the determination of ^{55}Fe and ^{63}Ni, a known quantity of the sample was transferred in a beaker, together with a known quantity of stable Carrier ($Fe(NO_3)_3{\cdot}9H_2O$ and ($Ni(NO_3)_2{\cdot}6H_2O$). The obtained sample was then centrifuged and chemical separation of ^{55}Fe was performed by means of TRU Resin (Triskem). The liquid discharged from TRU resin was evaporated and dissolved in a solution of Nitric Acid and Ammonium Citrate. The separation of ^{63}Ni was performed by NI-Resin (Triskem). In both the radiochemical separation for ^{55}Fe and ^{63}Ni the final solution was HNO_3 2 M.

Chemical recovery was assessed during the accreditation of the analytical methods, confirming a consistent recovery of approximately 90 % for both ^{55}Fe and ^{63}Ni under the conditions considered. As prescribed by the method, a control sample spiked with known activities of ^{55}Fe and ^{63}Ni was included in each analytical batch to verify that the chemical recovery remained within the expected range.

Then, the separated radionuclides were measured by liquid scintillation counting (LSC).

Instead, the characterization of ^{3}H was done by a controlled combustion process of a known quantity of the sample in a tube furnace (Carbolite GERO) with a constant flux of oxygen. A small amount of the sample was put in the furnace and then heated at 1000 °C for 2 h. The stripped ^{3}H, in form of gaseous $^{3}H_20$ was trapped in a recovery solution of Nitric acid 0.1 M and an aliquot of this solution was measured by LSC.

Chemical recovery was quantified based on analysis of a matrix-matched sample spiked with a certified tritium (^{3}H) standard.

The liquid scintillation measurement was performed using a Quantulus GCT-6220 (PerkinElmer). The efficiency calibration of this instrument was carried out by counting a quench curve for each of the three radionuclides, which allows to calculate the efficiency value for each sample (according to the Perkin Elmer tSIE value). The quench curve was made using a DAkkS certified solution by Eckert&Ziegler. The used analysis windows have been 0–6 keV for ^{55}Fe, 0–66 keV for ^{63}Ni and 0–18 keV for ^{3}H.

In a second phase the wall surface has been divided in a non-equispatial net (Fig. 5) with the most sampling concentrated in according to the FLUKA simulation and previous radiological characterization.

Samples, named 1–20 were taken by means of core drilling techniques (Fig. 6), to obtain samples related to different depth.

The 20 samples were first measured by means of gross beta (0–2000 keV) without chemical separation.

A blank sample, collected at the same site and chemically identical to the sample matrix, was prepared and processed following the same protocol as the analytical samples. Measurements were performed using LSC under identical conditions and counting times. The counts per minute (CPM) obtained from the blank was subtracted from the CPM of each sample to correct for background contributions.

This approach is a faster and economic way to verify the presence of beta emitters, and the results obtained from this screening can be correlated with a probable presence of ^{55}Fe, the only beta emitter that shows great activity concentration. However, this first step needs to be intended as a prior screening measure to verify the presence of radioactivity. It cannot be used to obtain the exact activity concentration of beta nuclides in the samples, because it is impossible to discriminate signals coming from different nuclides without performing a radiochemical separation.

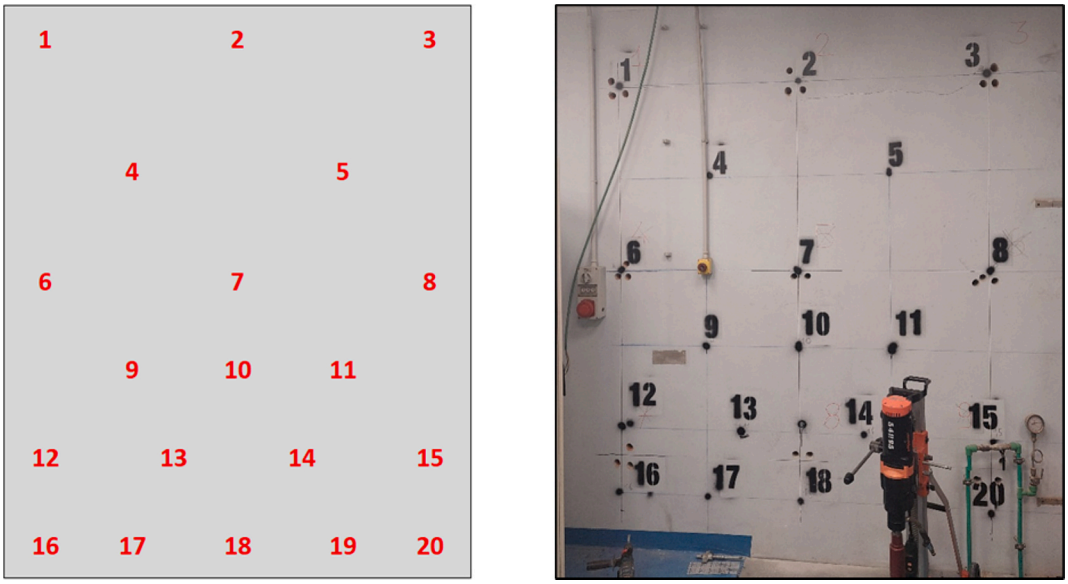

Fig. 5. Schematic representation and real outline of second sampling net.

Fig. 6. Sampling and sampled concrete cores.

The Minimum Detectable Counts per second (MDC) of this gross-beta analysis has been 0.02 cps g^{-1}.

In the samples with gross beta activity concentration greater than the MDC, the described above chemical separation of ^{55}Fe was performed.

2.3. Environmental and staff radioprotection and safety

Concerning environmental and staff radioprotection and safety, the decommissioning procedures were scheduled as shown in Table 1 [24].

This schedule calls for the preliminary dismantling of the easiest (in terms of the dismantling process) and hottest components (i.e., targets and vacuum Pumps) from the cyclotron after a brief waiting period after the last beam (Phase 1). The second step was to collect samples from the lateral wall of the cyclotron room by means of core drilling techniques. Finally, before the start of demolition operations a complete training program concerning the safety rules and procedures to be followed during the operation was carried out by the Radiation Protection Expert. In particular, as the demolition could represent a risk for inhalation of activated powders coming from the concrete, the main prescriptions regarding this operation were (i) that operating personnel were instructed to wear FFP3 masks and sealed suits to prevent radioactive dust inhalation and (ii) the use of a suitable drilling tool equipped with a vacuum pump and a dust collection tank was mandatory.

Table 1
Decommissioning and sampling program.

Phase #	Days after shutdown	Operations
0	Day 0 (09/09/2016)	Cyclotron shutdown
1	Day 30	Dismantling targets, vacuum pumps and cyclotron power supply by Hospital Engineers staff
2	Day 2800 (7 years and 8 months)	Samples taken from the wall by means of drilling in selected points
3	Day 2860 (7 years and 10 months)	Training course for demolition workers, wall demolition and cyclotron move out

The Medical Physics Department staff supervised all phases of the decommissioning, and collected radiation exposure data for both the

environment and the operating personnel:

- dose and dose-rate values in the operating room were measured using an organic scintillator probe (AUTOMESS 6150 ADB, ZnS-coated) for the real time measurement of the local background (minimum sensitivity 50 nSv h^{-1}, s.d. < 15 %);
- daily surface contamination tests on various employed tools (e.g., hammers, drills) as well as external (clothing) and internal (urine samples, spit and nasal mucus) tests for personnel were performed as described in [25], and measured by means of LSC or NaI gamma counter (LKB Wallac energy resolution = 8.4 keV and efficiency = 9 % at 661 keV of ^{137}Cs).

3. Results and discussion

3.1. Concrete wall results

3.1.1. FLUKA simulations

Using the FLUKA simulation, the results presented in Fig. 7 were obtained. The simulation demonstrates that the highest activity is found in the top layer (0–5 cm), with approximately 99 % of the total activity concentration confined to the first 40 cm, and beyond this depth, the ^{55}Fe activity falls below 1 Bq g^{-1} (Italian clearance level [18]).

3.1.2. Experimental measurements

Measurements of gamma emitters were conducted on concrete wall samples extracted from nine points arranged in a 3 x 3 m^2 grid within the demolition area (Fig. 4), reaching a depth of up to 30 cm.

The results of these first nine samples are reported in Table 2.

Beta spectrometry analysis using liquid scintillation was performed on the same samples (Table 3).

Samples 7old, 8old, 9old, located in the lower part of the concrete wall, show ^{55}Fe activity concentrations three and four times above the clearance level (1 Bq g^{-1}). In these samples only ^{55}Fe was found above the clearance level, ^{63}Ni has only a point slightly above clearance, that is statistically unsignificant; others beta emitters were found only in traces.

In samples 1old to 6old, only ^{63}Ni was detected with activity concentrations consistently above the minimum detectable activity (MDA), although well below the clearance level. Neither ^{55}Fe nor ^{3}H were detected in these samples, with values remaining below the detection thresholds (Fig. 8).

Therefore, it was decided to carry out an additional 20 samplings (Fig. 5) with focus on middle and lower part of the wall and to divide each sample into 3 layers (A-layer, 0–5 cm; B-layer, 5–30 cm; C-layer, >30 cm).

First, a screening measurement of total activity for beta-emitting radionuclides (gross-beta measurement) was conducted on these new samples (Fig. 9).

Instead, in the layer 0–5 cm (named A-layer) analysis show the most presence of activity concentration with values above the gross-beta MDC (0.02 cps g^{-1}): as expected, most samples with high activity concentration (from 15 to 20, see Fig. 5) were in the middle-lower side of the wall.

Other net signals were found in layer A (1, 3, 5, 10, and 13) and layer B (12, 16, 17, 18, and 19) too.

To confirm the screening measures, on samples with activity concentration above the MDC, the quantification of ^{55}Fe was performed (Table 4).

No ^{55}Fe signal was found in samples taken at a depth greater than 5 cm (named B-layer and C-layer). Instead, in the layer 0–5 cm (named A-layer) the activity concentration of ^{55}Fe is below the clearance level in samples 1, 3, 5, 10, 13, and 17 and above the clearance level in samples

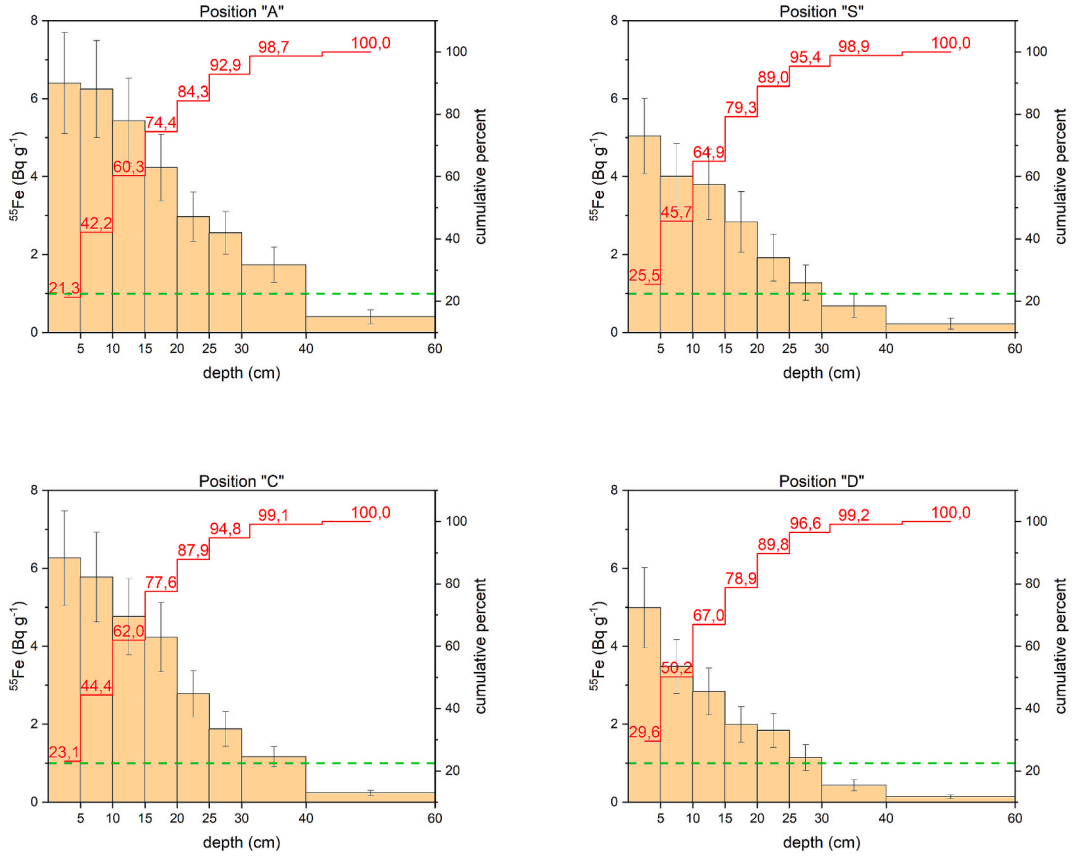

Fig. 7. ^{55}Fe distribution in the simulated samples and layers. The green dashed line represents the clearance level for Italian legislation (1 Bq·g^{-1}). (For interpretation of the references to colour in this figure legend, the reader is referred to the web version of this article.)

Table 2
Radioactivity concentration of the gamma emitter radionuclides in concrete wall sampling 1old-9old. Where characteristic gamma emissions are not evident, the value of the Minimum Detectable Activity (<MDA) has been indicated.

	Radioactivity concentration (Bq g^{-1})								
	1old	2old	3old	4old	5old	6old	7old	8old	9old
^{60}Co	$<6 \times 10^{-5}$	$26 \times 10^{-5} \pm 11 \times 10^{-5}$	$21 \times 10^{-5} \pm 10 \times 10^{-5}$	$27 \times 10^{-5} \pm 9 \times 10^{-5}$	$<7 \times 10^{-5}$	$21 \times 10^{-5} \pm 8 \times 10^{-5}$	$13 \times 10^{-5} \pm 6 \times 10^{-5}$	$33 \times 10^{-5} \pm 12 \times 10^{-5}$	$24 \times 10^{-5} \pm 11 \times 10^{-5}$
^{134}Cs	$<5 \times 10^{-5}$	$<7 \times 10^{-5}$	$<6 \times 10^{-5}$	$<6 \times 10^{-5}$	$<5 \times 10^{-5}$	$<5 \times 10^{-5}$	$<5 \times 10^{-5}$	$<5 \times 10^{-5}$	$<5 \times 10^{-5}$
^{137}Cs	$45 \times 10^{-5} \pm 7 \times 10^{-5}$	$55 \times 10^{-5} \pm 9 \times 10^{-5}$	$58 \times 10^{-5} \pm 8 \times 10^{-5}$	$16 \times 10^{-5} \pm 7 \times 10^{-5}$	$70 \times 10^{-5} \pm 6 \times 10^{-5}$	$<6 \times 10^{-5}$	$<6 \times 10^{-5}$	$<6 \times 10^{-5}$	$<6 \times 10^{-5}$
^{152}Eu	$<3 \times 10^{-4}$	$<4 \times 10^{-4}$	$<4 \times 10^{-4}$	$<4 \times 10^{-4}$	$<3 \times 10^{-4}$	$<3 \times 10^{-4}$	$<3 \times 10^{-4}$	$<3 \times 10^{-4}$	$<3 \times 10^{-4}$
^{154}Eu	$<2 \times 10^{-4}$	$<3 \times 10^{-4}$	$<2 \times 10^{-4}$	$<2 \times 10^{-4}$	$<2 \times 10^{-4}$	$<2 \times 10^{-4}$	$<2 \times 10^{-4}$	$<2 \times 10^{-4}$	$<2 \times 10^{-4}$
^{40}K	$48 \times 10^{-2} \pm 3 \times 10^{-2}$	$68 \times 10^{-2} \pm 4 \times 10^{-2}$	$66 \times 10^{-2} \pm 3 \times 10^{-2}$	$52 \times 10^{-2} \pm 3 \times 10^{-2}$	$42 \times 10^{-2} \pm 2 \times 10^{-2}$	$43 \times 10^{-2} \pm 2 \times 10^{-2}$	$49 \times 10^{-2} \pm 3 \times 10^{-2}$	$28 \times 10^{-2} \pm 2 \times 10^{-2}$	$44 \times 10^{-2} \pm 2 \times 10^{-2}$
^{214}Pb	$37 \times 10^{-3} \pm 3 \times 10^{-3}$	$63 \times 10^{-3} \pm 5 \times 10^{-3}$	$62 \times 10^{-3} \pm 5 \times 10^{-3}$	$40 \times 10^{-3} \pm 3 \times 10^{-3}$	$27 \times 10^{-3} \pm 2 \times 10^{-3}$	$27 \times 10^{-3} \pm 2 \times 10^{-3}$	$35 \times 10^{-3} \pm 3 \times 10^{-3}$	$28 \times 10^{-3} \pm 2 \times 10^{-3}$	$18.2 \times 10^{-3} \pm 1.3 \times 10^{-3}$
^{214}Bi	$30 \times 10^{-3} \pm 2 \times 10^{-3}$	$49 \times 10^{-3} \pm 3 \times 10^{-3}$	$49 \times 10^{-3} \pm 3 \times 10^{-3}$	$31 \times 10^{-3} \pm 2 \times 10^{-3}$	$20.8 \times 10^{-3} \pm 1.4 \times 10^{-3}$	$21.2 \times 10^{-3} \pm 1.4 \times 10^{-3}$	$28 \times 10^{-3} \pm 2 \times 10^{-3}$	$21.0 \times 10^{-3} \pm 1.3 \times 10^{-3}$	$15.1 \times 10^{-3} \pm 0.9 \times 10^{-3}$
^{228}Ac	$30 \times 10^{-3} \pm 2 \times 10^{-3}$	$55 \times 10^{-3} \pm 4 \times 10^{-3}$	$55 \times 10^{-3} \pm 3 \times 10^{-3}$	$34 \times 10^{-3} \pm 2 \times 10^{-3}$	$20.3 \times 10^{-3} \pm 1.3 \times 10^{-3}$	$22.1 \times 10^{-3} \pm 1.4 \times 10^{-3}$	$29 \times 10^{-3} \pm 2 \times 10^{-3}$	$19.2 \times 10^{-3} \pm 0.9 \times 10^{-3}$	$15.8 \times 10^{-3} \pm 0.8 \times 10^{-3}$
^{212}Pb	$44 \times 10^{-3} \pm 4 \times 10^{-3}$	$81 \times 10^{-3} \pm 7 \times 10^{-3}$	$79 \times 10^{-3} \pm 7 \times 10^{-3}$	$51 \times 10^{-3} \pm 4 \times 10^{-3}$	$31 \times 10^{-3} \pm 3 \times 10^{-3}$	$34 \times 10^{-3} \pm 3 \times 10^{-3}$	$44 \times 10^{-3} \pm 4 \times 10^{-3}$	$31 \times 10^{-3} \pm 3 \times 10^{-3}$	$20 \times 10^{-3} \pm 2 \times 10^{-3}$
^{235}U	$22 \times 10^{-4} \pm 2 \times 10^{-4}$	$45 \times 10^{-4} \pm 5 \times 10^{-4}$	$35 \times 10^{-4} \pm 5 \times 10^{-4}$	$44 \times 10^{-4} \pm 2 \times 10^{-4}$	$17 \times 10^{-4} \pm 2 \times 10^{-4}$	$19 \times 10^{-4} \pm 2 \times 10^{-4}$	$21 \times 10^{-4} \pm 2 \times 10^{-4}$	$18 \times 10^{-4} \pm 2 \times 10^{-4}$	$7 \times 10^{-4} \pm 1 \times 10^{-4}$
^{226}Ra	$28 \times 10^{-3} \pm 11 \times 10^{-3}$	$49 \times 10^{-3} \pm 7 \times 10^{-3}$	$48 \times 10^{-3} \pm 8 \times 10^{-3}$	$30 \times 10^{-3} \pm 7 \times 10^{-3}$	$22 \times 10^{-3} \pm 4 \times 10^{-3}$	$29 \times 10^{-3} \pm 5 \times 10^{-3}$	$26 \times 10^{-3} \pm 5 \times 10^{-3}$	$24 \times 10^{-3} \pm 7 \times 10^{-3}$	$23 \times 10^{-3} \pm 7 \times 10^{-3}$
^{208}Tl	$116 \times 10^{-4} \pm 8 \times 10^{-4}$	$207 \times 10^{-4} \pm 14 \times 10^{-4}$	$201 \times 10^{-4} \pm 14 \times 10^{-4}$	$121 \times 10^{-4} \pm 8 \times 10^{-4}$	$72 \times 10^{-4} \pm 5 \times 10^{-4}$	$80 \times 10^{-4} \pm 6 \times 10^{-4}$	$104 \times 10^{-4} \pm 7 \times 10^{-4}$	$72 \times 10^{-4} \pm 5 \times 10^{-4}$	$54 \times 10^{-4} \pm 4 \times 10^{-4}$
^{212}Bi	$33 \times 10^{-3} \pm 2 \times 10^{-3}$	$61 \times 10^{-3} \pm 4 \times 10^{-3}$	$64 \times 10^{-3} \pm 4 \times 10^{-3}$	$40 \times 10^{-3} \pm 3 \times 10^{-3}$	$25 \times 10^{-3} \pm 2 \times 10^{-3}$	$28 \times 10^{-3} \pm 2 \times 10^{-3}$	$33 \times 10^{-3} \pm 2 \times 10^{-3}$	$22 \times 10^{-3} \pm 2 \times 10^{-3}$	$20 \times 10^{-3} \pm 2 \times 10^{-3}$
^{234}Th	$2.9 \times 10^{-2} \pm 0.3 \times 10^{-2}$	$4.4 \times 10^{-2} \pm 0.5 \times 10^{-2}$	$4.6 \times 10^{-2} \pm 0.4 \times 10^{-2}$	$3.4 \times 10^{-2} \pm 0.4 \times 10^{-2}$	$2.1 \times 10^{-2} \pm 0.4 \times 10^{-2}$	$2.4 \times 10^{-2} \pm 0.4 \times 10^{-2}$	$2.0 \times 10^{-2} \pm 1.2 \times 10^{-2}$	$3.1 \times 10^{-2} \pm 0.5 \times 10^{-2}$	$<7 \times 10^{-3}$

Table 3
Radioactivity concentration of the beta emitter radionuclides in concrete wall sampling 1old-9old.

	Activity concentration (Bq g^{-1})								
	1old	2old	3old	4old	5old	6old	7old	8old	9old
^{55}Fe	<0.7	<0.6	<0.7	<0.9	<0.9	<0.7	2.72 ± 0.66	4.64 ± 0.86	4.46 ± 0.78
^{63}Ni	0.37 ± 0.11	0.40 ± 0.12	0.42 ± 0.13	0.31 ± 0.10	0.22 ± 0.07	0.09 ± 0.04	0.20 ± 0.07	0.55 ± 0.17	1.7 ± 0.5
^{3}H	<0.03	<0.03	<0.03	<0.03	0.10 ± 0.03	<0.03	<0.03	<0.06	<0.06

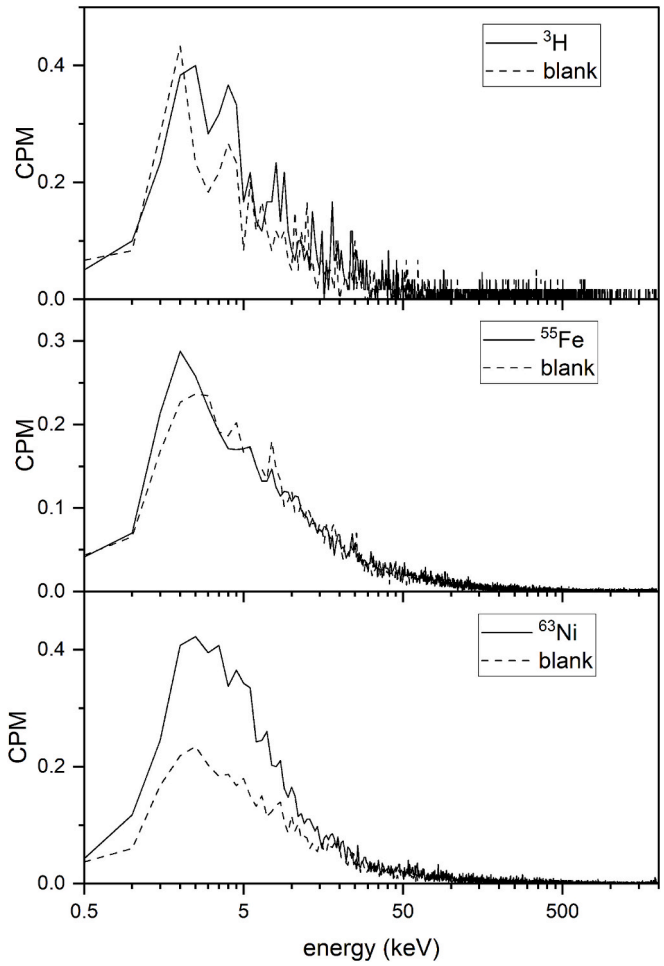

Fig. 8. Beta spectra for ^{3}H, ^{55}Fe, and ^{63}Ni from sample 3old.

15, 16, 18, 19, and 20 with maximum value of around 10 Bq g^{-1} (15-A and 20-A).

The net signal shown by the beta-gross screening in the B-Layer is probably due to interferences caused by other beta emitter radionuclides such ^{40}K, uranium series beta emitters, thorium series beta emitters, by the potential presence of $^{59/63}$Ni or other phenomena such chemiluminescence effects.

The compatibility between FLUKA simulations and experimental measurements, each with associated uncertainties, was assessed using normalized deviations and a chi-squared test. For all data pairs, the normalized differences were within ±2, indicating individual compatibility. The global agreement was evaluated using the chi-squared statistic. With 4 degrees of freedom, $\chi^2 = 8.12$ and a p-value of 0.087. Since the p-value exceeds the commonly accepted threshold of 0.05, we conclude that there is no statistically significant incompatibility between the two datasets.

It can be concluded that the presence of ^{55}Fe is detectable only in the A-Layer (0–5 cm) with the highest concentration in the lower part of the wall.

3.1.3. *Demolition staff external doses and intake results*

The last subject explored in both predictive and post-operational mode was the dose to personnel involved in the wall demolition.

3.1.3.1. Preventive checks. The measured dose rates on both sides of the operational area (inside the cyclotron vault and outside in the corridor zone) confirm a value comparable to the background (0.15 μSv h^{-1}).

Therefore, the Radiation Safety Officer predicted a null value both for the external exposure and for the contamination dose of the involved staff.

Nevertheless, each member of the staff was equipped with a sealed suit and filtered mask (FFP3) during operations and a personal electronic dosemeter (Rados, mod. Rad60).

3.1.3.2. Post operational results. The demolition of the part of the wall (60 cm thick, 250 × 250 cm^2 brick) needed for the extraction of the cyclotron, took seven working days and was carried out by a team of three bricklayers equipped with water-cooled pneumatic hammers (Fig. 10).

Daily the individual external doses were measured by means of electronic personal dosimeters and the internal contamination of the staff was analysed collecting nasal mucus and saliva samples by means of beta counter Perkin ElmerTricarb 2810 TR 35366 with a sampling volume of 5 ml filled with 3 cc of scintillation liquid, calibrated at ^{3}H energy with an MDA value equal to 0.7 Bq ml^{-1}, absolute efficiency 18 %, in a counting time of 3 min. All the collected samples, taken at the end of every working day at the bricklayers' staff, have not revealed values above the background (average 2.2 CPM, standard deviation 1.2 CPM).

Nevertheless, the inhaled amount of ^{55}Fe corresponding to a committed dose of 1 μSv would be 1.087 × 10^{3} Bq [26]. Considering that in our concrete we should have a concentration value of the order of 1

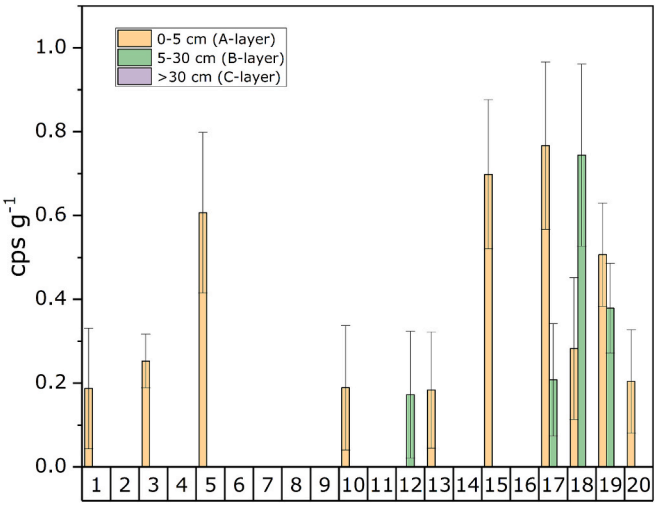

Fig. 9. Gross-beta measurement for all the samples and layers.

Table 4
^{55}Fe activity concentration.

Sample ID			^{55}Fe (Bq g^{-1})
1	–	A	0.4 ± 0.2
3	–	A	0.4 ± 0.2
5	–	A	<0.2
10	–	A	0.20 ± 0.16
12	–	B	<0.2
13	–	A	0.7 ± 0.2
15	–	A	10.6 ± 1.0
16	–	A	2.4 ± 0.4
16	–	B	<0.2
17	–	A	0.7 ± 0.2
17	–	B	<0.2
18	–	A	3.3 ± 0.5
18	–	B	<0.2
19	–	A	4.0 ± 0.7
19	–	B	<0.2
20	–	A	10.4 ± 1.4

Fig. 10. The demolition of the wall.

Bq g^{-1} it would correspond to an inhalation amount of 1 kg of powders with a mucosa deposition of 0.38 kg [26] that is roughly 400 Bq. Therefore, we can assess that the sensitivity of the measure with an MDA of 0.7 Bq ml^{-1} is appropriate for the detection limit of an intake corresponding to an effective committed dose of 1 μSv. Both types of measurements brought null value for all the members of the staff throughout the entire period of operation.

4. Conclusions

The decommissioning of the 11 MeV self-shielded cyclotron was executed with a methodical and multidisciplinary approach, combining computational modelling, laboratory validation, and stringent radioprotection protocols. FLUKA simulations predicted a clear depth-dependent distribution of neutron-induced activation, a result that was corroborated by direct experimental measurements. Specifically, the simulations and measurements identified ^{55}Fe as the dominant long-lived activation product, with significant activity concentrations localized within the first 5 cm of the surface layer of the cyclotron vault wall, especially in its lower sections.

The effective implementation of radiochemical separation techniques and low-level beta liquid scintillation spectrometry enabled precise quantification of ^{55}Fe and ^{63}Ni, ensuring that assessments adhered to Italian clearance levels. Notably, several wall sections exceeded the national regulatory threshold for ^{55}Fe and ^{63}Ni, underscoring the need for partial classification as radioactive waste. However, in comparison with clearance thresholds set by other European [27] regulations (e.g., French [28], Spanish [29], German [30,31]), these values remain well within acceptable margins, suggesting a potentially more flexible waste categorization under different regulatory contexts.

From a radioprotection standpoint, the operations were managed with exemplary safety procedures. Personnel involved in the demolition were equipped with protective suits, filtered masks, and personal dosimeters. Both external dose measurements and internal contamination checks returned values below the limits of detection, validating the efficacy of the protective measures and confirming that the operation posed negligible health risk to staff.

In conclusion, this work demonstrates the critical importance of coupling predictive simulation with empirical validation in radiation safety management. The careful planning and execution of the decommissioning ensured regulatory compliance and minimized environmental and occupational hazards. The findings also contribute valuable data to the growing body of literature on the activation of cyclotron vault materials, aiding future decommissioning projects in both medical and research contexts. The identified presence of long-lived radionuclides necessitates continued attention to waste classification and long-term storage protocols, ensuring safety not just during decommissioning, but also throughout the lifecycle of waste management.

Declaration of Generative AI and AI-assisted technologies in the writing process

During the preparation of this work the authors used OpenAI's ChatGPT in order to develop and refine of this paper. After using this tool, the authors reviewed and edited the content as needed and take full responsibility for the content of the publication.

Declaration of competing interest

The authors declare the following financial interests/personal relationships which may be considered as potential competing interests: Carlo Bergamaschi reports a relationship with Campoverde srl that includes: employment. Andrea Ferrari reports a relationship with Campoverde srl that includes: employment. Massimiliano Nizzi reports a relationship with Campoverde srl that includes: employment. If there are other authors, they declare that they have no known competing financial interests or personal relationships that could have appeared to influence the work reported in this paper.

References

[1] Calandrino R, Del Vecchio A, Savi A, Todde S, Griffoni V, Brambilla S, et al. Decommissioning procedures for an 11 MeV self-shielded medical cyclotron after 16 years of working time. Health Phys 2006;90(6):588–96. https://doi.org/10.1097/01.HP.0000190161.96172.ae.
[2] Birattari C, Cantone MC, Ferrari A, Silari M. Residual radioactivity at the Milan AVF cyclotron. Nucl Instrum Methods Phys Res, Sect B 1989;43(1):119–26. https://doi.org/10.1016/0168-583X(89)90090-6.
[3] Bonvin V, Bochud F, Damet J, Theis C, Vincke H, Geyer R. Detailed study of the distribution of activation inside the magnet coils of a compact PET cyclotron. Appl Radiat Isot 2021;168:109446. https://doi.org/10.1016/j.apradiso.2020.109446.
[4] Hermanne A, Eggermont G. Decommissioning and Nuclear Waste Analysis of a University Cyclotron. In: GRC Conference on Nuclear Waste Energy. Prague, Czech Republic; 1996.
[5] Silari M. Special radiation protection aspects of medical accelerators. Radiat Prot Dosim 2001;96(4):381–92. https://doi.org/10.1093/oxfordjournals.rpd.a006626.
[6] Toyoda A, Yoshida G, Matsumura H, Masumoto K, Nakabayashi T, Yagishita T, et al. Evaluation of induced activity in various components of a PET-cyclotron.

J Phys Conf Ser 2018;1046:12017. https://doi.org/10.1088/1742-6596/1046/1/012017.
[7] Carroll LR. Predicting long-lived, neutron-induced activation of concrete in a cyclotron vault. AIP Conference Proceedings AIP 2001:301–4.
[8] Kimura K, Ishikawa T, Kinno M, Yamadera A, Nakamura T. Residual long-lived radioactivity distribution in the inner concrete wall of a cyclotron vault. Health Phys 1994;67(6):621–31. https://doi.org/10.1097/00004032-199412000-00005.
[9] Phillips AB, Prull DE, Ristinen RA, Kraushaar JJ. Residual radioactivity in a cyclotron and its surroundings. Health Phys 1986;51(3).
[10] Sonck M, Buls N, Hermanne A, Eggermont G. Radiological and economic impact of decommissioning charged particle accelerators. Japan Health Physics Society 2025.
[11] Vichi S, Infantino A, Zagni F, Cicoria G, Braccini S, Mostacci D, et al. Activation studies for the decommissioning of PET cyclotron bunkers by means of Monte Carlo simulations. Radiat Phys Chem 2020;174:108966. https://doi.org/10.1016/j.radphyschem.2020.108966.
[12] Pola A, Bortot D, Pasquato S, Mazzucconi D, Chiesa C, Zanellati F, et al. Decommissioning of a medical cyclotron vault: the case study of the National Cancer Institute of Milano. Health Phys 2024;127(2):276–86. https://doi.org/10.1097/HP.0000000000001801.
[13] Bungau C, Bungau A, Cywinski R, Barlow R, Edgecock TR, Carlsson P, et al. Induced activation in accelerator components. Phys Rev ST Accel Beams 2014;17(8). https://doi.org/10.1103/PhysRevSTAB.17.084701.
[14] Blaha J, La Torre FP, Silari M, Vollaire J. Long-term residual radioactivity in an intermediate-energy proton linac. Nucl Instrum Methods Phys Res, Sect A 2014;753:61–71. https://doi.org/10.1016/j.nima.2014.03.058.
[15] Urabe I, Kobayashi K, Fujita Y, Tsujimoto T, Jin GC. Depth distribution of residual radioactivities in the concrete wall of an electron linac facility. Health Phys 1991;60(4):587–91. https://doi.org/10.1097/00004032-199104000-00016.
[16] Hermanne A. Decommissioning medical linear accelerators: a study on identification and minimization of nuclear waste. Antwerp 1999.
[17] Calandrino R, Manenti S, Groppi F, Broggi F, Bergamaschi C, Ferrari A, et al. Decommissioning procedure and induced activation levels, calculations and measurements in an 18 MeV medical cyclotron. J Radiol Prot 2021;41(4). https://doi.org/10.1088/1361-6498/ac28f0.
[18] Repubblica Italiana. Decreto Legislativo n. 101/2020 – Attuazione della direttiva 2013/59/Euratom in materia di protezione dalle radiazioni ionizzanti; 2020.
[19] Ahdida C, Bozzato D, Calzolari D, Cerutti F, Charitonidis N, Cimmino A, et al. New capabilities of the FLUKA Multi-purpose code. Front Phys 2022;9. https://doi.org/10.3389/fphy.2021.788253.
[20] Battistoni G, Boehlen T, Cerutti F, Chin PW, Esposito LS, Fassò A, et al. Overview of the FLUKA code. Ann Nucl Energy 2015;82:10–8. https://doi.org/10.1016/j.anucene.2014.11.007.
[21] Vlachoudis V. Flair: A powerful but user friendly graphical interface for FLUKA. In: International Conference on Mathematics, Computational Methods & Reactor Physics 2009; 2009, p. 790–800.
[22] Eichrom Technologies LLC. FEW01 – Analytical Procedure for Fe-55. Lisle, IL, USA; 2014.
[23] Eichrom Technologies LLC. NIW01 – Analytical Procedure for Ni-63. Lisle, IL, USA; 2014.
[24] International Atomic Energy Agency. Specific Safety Guide No. SSG-49. Vienna, Austria; 2019.
[25] Calandrino R, Del Vecchio A, Savi A, Todde S, Belloli S. Intake risk and dose evaluation methods for workers in radiochemistry labs of a medical cyclotron facility. Health Phys 2009;97(4):315–21. https://doi.org/10.1097/HP.0b013e3181ad8192.
[26] International Commission on Radiological Protection. Dose Coefficients for Intakes of Radionuclides by Workers. Oxford, UK: Pergamon Press; 1994.
[27] European Council. Council Directive 2013/59/EURATOM: Laying down basic safety standards for protection against the dangers arising from exposure to ionising radiation; 2013.
[28] République Française. Ordonnance n° 2016-128 du 10 février 2016 portant diverses dispositions en matière nucléaire; 2016.
[29] Reino de España. Real Decreto 1029/2022, de 20 de diciembre, por el que se establecen los criterios de protección sanitaria frente a los riesgos derivados de las radiaciones ionizantes; 2022.
[30] Bundesrepublik Deutschland. Strahlenschutzgesetz (StrlSchG) - German Radiation Protection Act; 2017.
[31] Bundesrepublik Deutschland. Strahlenschutzverordnung (StrlSchV) - German Radiation Protection Ordinance; 2018.